Environmental Science Nano

ROYAL SOCIETY OF CHEMISTRY

PAPER

View Article Online
View Journal | View Issue

Cite this: *Environ. Sci.: Nano*, 2025, 12, 660

Nanocarrier foliar uptake pathways affect delivery of active agents and plant physiological response†

Hagay Kohay, [a] Jonas Wielinski, [a] Jana Reiser,[a] Lydia A. Perkins,[b] Kurt Ristroph,[ce] Juan Pablo Giraldo [d] and Gregory V. Lowry *[a]

Layered double hydroxide (LDH) nanoparticles enable foliar delivery of genetic material, herbicides, and nutrients to promote plant growth and yield. Understanding the foliar uptake route of nanoparticles is needed to maximize their effectiveness and avoid unwanted negative effects. In this study, we investigated how delivering layered double hydroxide (d = 37 ± 1.5 nm) through the adaxial (upper) or abaxial (lower) side of leaves affects particle uptake, nutrient delivery, and photosynthesis in tomato plants. LDH applied on the adaxial side was embedded in the cuticle and accumulated at the anticlinal pegs between epidermal cells. On the abaxial side, LDH particles penetrated the cuticle less, but the presence of the stomata enables penetration to deeper leaf layers. Accordingly, the average penetration levels of LDH relative to the cuticle were 2.47 ± 0.07, 1.25 ± 0.13, and 0.75 ± 0.1 μm for adaxial, abaxial with stomata, and abaxial without stomata leaf segments, respectively. In addition, the colocalization of LDH with the cuticle was ~2.3 times lower for the adaxial application, indicating the ability to penetrate the cuticle. Despite the low adaxial stomata density, LDH-mediated delivery of magnesium (Mg) from leaves to roots was 46% higher for the adaxial than abaxial application. In addition, adaxial application leads to ~24% higher leaf CO_2 assimilation rate and higher biomass accumulation. The lower efficiency from the abaxial side was, at least partially, a result of interference with the stomata functionality which reduced stomatal conductance and evapotranspiration by 28% and 25%, respectively, limiting plant photosynthesis. This study elucidates how foliar delivery pathways through different sides of the leaves affect their ability to deliver active agents into plants and consequently affect the plants' physiological response. That knowledge enables a more efficient use of nanocarriers for agricultural applications.

Received 17th June 2024,
Accepted 9th October 2024

DOI: 10.1039/d4en00547c

rsc.li/es-nano

Environmental significance

Nanomaterials can enhance the utilization efficiency and efficacy of agrochemicals and minimize the environmental impacts of agriculture. However, a mechanistic understanding of how nanoparticles interact with, penetrate, and move into plant leaves is needed to take full advantage of nanotechnology. Here, we imaged and analyzed the foliar uptake routes and the resulting physiological responses in tomato plants for ~35 nm layered double hydroxides, a proposed nanocarrier for agriculture. The findings from this study can be used to design more precise pest and weed management strategies and delivery of nucleic acids, thereby increasing use efficiency and reducing the environmental burden of agriculture.

Introduction

Foliar application of nanocarriers (NC) can improve the active agents (AA) delivery efficiency into plants.[1] NC have the potential to improve the association of the AA with the leaves and therefore to enhance the rain fastness,[2] control the release rate of AA,[3] enhance the mobility of the AA in the plant,[4] and protect the AA from degradation.[5] Foliar application of AA in NC is an attractive approach to increase utilization efficiency compared to soil application, with a lower amount of nutrients or AA being wasted and leached into soils and receiving waters; thus, reducing adverse impacts on non-target organisms. However, NC uptake into the leaves can be inefficient. For example, Rodrigues *et al.*, 2024 (ref. 6) reported that less than 7% of the zinc oxide-based materials applied to pepper leaves were taken up by the

[a] *Carnegie Mellon University, Civil & Environmental Engineering, Pittsburgh, PA, USA. E-mail: glowry@andrew.cmu.edu*
[b] *Molecular Biosensor & Imaging Center (MBIC), Carnegie Mellon University, Pittsburgh, PA, USA*
[c] *Purdue University, Agricultural & Biological Engineering, West Lafayette, IN, USA*
[d] *University of California, Botany & Plant Sciences, Riverside, Riverside, CA, USA*
[e] *Purdue University, Davidson School of Chemical Engineering, West Lafayette, IN, USA*
† Electronic supplementary information (ESI) available. See DOI: https://doi.org/10.1039/d4en00547c

leaves. Particles' size, charge, and surface chemistry were reported to affect the NC ability to interact with the leaf interfaces[7] affecting NP uptake.[8–11] To improve uptake efficiency, the factors controlling NC-leaf interactions, including how anatomical differences between the adaxial and abaxial sides of the leaves affect the uptake routes, need to be better understood.[12,13]

Different types of NC are being used to improve AA delivery. They can be divided into NC made of the AA itself (such as Zinc (Zn) or Copper (Cu) Oxides) or NC loaded with an AA,[14] which are often made from polymers, peptides, silica, and carbon. In many cases, NC is suitable for a specific goal based on its properties. However, for extending its use, an essential property of NC is its versatility; in that term, LDH is an interesting material for foliar delivery since its physiochemical properties such as size, charge, and surface characteristics can be tuned to enhance uptake into leaves.[15] LDH can be formulated to use as a carrier for different agrochemicals. It was reported as a potential NC for the delivery of nutrients embedded in its structure (magnesium (Mg), Zn, Cu, Iron (Fe))[16–18] as well as a carrier of organic or inorganic AA molecules.[19,20] LDH is considered a bio-compatible[21,22] and food-compatible material[23] and can ultimately be degraded under environmental conditions. The stability of LDH is controlled by the pH of the solution,[24] which suggests that the release of the AA inside of plants will depend on the pH of the target regions, *e.g.* cytosol *vs.* apoplast. While the pH in the cytosol (symplast) is neutral (6.8–7.2), the pH in the apoplast and vacuole is more acidic (5.5–6),[25,26] which will promote a more rapid dissolution. A prior study using Mg-Al LDH as a carrier of the herbicide 2-methyl-4-chlorophenoxyacetate showed a higher release rate as pH was reduced.[27] LDH has previously been used as a carrier for foliar application, for example: an LDH-2,4 D complex demonstrated slow release of the herbicide and a stronger herbicide effect compared to the free 2,4 D.[28] Recently, LDH was investigated as a platform to stabilize and deliver short sequences of RNA for plant protection against viruses[3] and insects.[29] Yong J. *et al.*, 2022 studied the localization of LDH upon infiltration from the abaxial side of *B. Nicotiana* and demonstrated its ability to deliver siRNA.[30] To promote a wider and more efficient utilization of LDH for nutrients and AA delivery in agrochemical applications, a better understanding of LDH-leaf interactions is needed.

The two main uptake routes most often reported for NC into a leaf surface are the stomata and cuticle.[10] However, trichomes and hydathodes have also been suggested as potential uptake routes for NC and nanoparticles (NP).[10,31,32] These latter two routes are less well studied. The density of stomata and the cuticle properties are different on the adaxial and abaxial sides of the leaf, which we hypothesized would affect the uptake of NC, such as LDH and their cargo. When open, the stomata (3–10 μm) do not pose size limitations for the entrance of NC, and have been suggested as the main route for uptake.[22,33–35] The cuticle, the hydrophobic barrier of the leaf surface, is composed of a combination of materials such as cutin, cutan, waxes, polysaccharides, and phenolics.[36] The cuticle covers most of the leaf surface and can have a substantial effect on NC-leaf interactions. Because of the differences in the cuticle properties, NC uptake is expected to vary between plant species as well as between adaxial and abaxial applications in the same plant. For tomatoes, which were tested in this study, the abaxial side consists of a higher stoma and trichome density compared to the adaxial side. Henningsen *et al.*, 2023, reported stomata density of 189 ± 5.1 and trichome density of 83.7 ± 2.4 on the abaxial side of tomato leaves *vs.* 1.8 ± 0.6 stomata per mm^2 and 16.5 ± 0.8 trichomes per mm^2 for the adaxial side.[37] The much higher density of stomata on the abaxial side of the leaf is expected to promote the uptake of NC. On the other hand, the adaxial side is more wettable, which allows for better dispersion and interaction of the NC with the leaf surface.[37] Recently, Gao *et al.*, demonstrated an improved uptake and translocation of ZnO Nanoparticles Encapsulated in Mesoporous silica when applied on the abaxial side supporting stomata as the primary uptake pathway.[13] The stomata were found as the main entrance route for Zn oxide applied to wheat leaves.[12] Additional factors can also affect the interactions; for example, the solution composition, including surfactants or other additives, can impair the cuticle integrity and promote uptake. In addition, the spraying conditions (*e.g.*, nozzle/drop size, spray velocity, adjuvant type) and physiological state of the plant at the time of spraying (*e.g.*, if stomata are open or closed) can affect NC uptake. Efficient application of LDH as NC requires a comprehensive understanding of uptake pathways and an examination of the LDH impact on plant health.

NC may either promote or restrain plant growth and yield. To improve plant performance, NC must provide for a specific need of the plant (*e.g.* supply a needed nutrient,[38] reduce stress,[39] *etc.*), and deliver that agent to the correct location and at the appropriate rate.[40,41] If these conditions are not met, the addition of NC might impair plant growth.[42] In addition to these factors, NC are known to elicit the plants' defence mechanisms, which can promote plant performance under stress.[43] All the above factors contribute to the overall effect of the NC. LDH was used here as a case study to elucidate the interplay between the uptake pathway and the effect on the physiological status of the plant. Mg plays a significant role in plant growth (central metal in chlorophyll, cofactor in many enzymes, protein production, and more).[44,45] Because Mg can independently translocate in the plant upon dissolution of the LDH NP,[46] the interplay between uptake pathways and physiological status can be investigated and potentially generalized to other cases.

In this study, we present a method to synthesize small LDH particles (~37 nm) for use as NC. We characterized the LDH association and coverage on the external surfaces of the leaf, and the penetration level into the leaf through both cuticle and stomata. In addition, we tested how foliar application of LDH on the leaf surfaces affects biomass

accumulation, Mg translocation, and photosynthetic efficiency. This study contributes to the basic understanding of the biophysical processes of LDH uptake by the leaf and the related response of the plant. This knowledge can be utilized to design effective LDH-based agrochemical carriers and to improve NC delivery for a more sustainable agrochemical practice.

Materials and methods

Materials

$Mg(NO_3)_2{\cdot}6H2O$, tris(hydroxymethyl)aminomethane (THAM), $TbCl_3{\cdot}6H2O$, auramine O and amicon Ultra-4 10 kDa centrifugal filters were purchased from Sigma. 15× A/T ssDNA-Cy3 was purchased from IDT, H-PTFH filters 0.45 μm were purchased from Whatman, and standard RC tubing MWCO 6–8 kD#1 was purchased from spectra/Por.

LDH preparation and modification

For the aqueous procedure, L-LDH and S-LDH were synthesized in the presence of tris(hydroxymethyl) aminomethane (THAM) based on[47] with modifications. The basic procedure for L-LDH synthesis was to mix the metal solution consisting of 7.5 mL of 2.5 mmol of Mg : Al : Tb at a molar ratio of 3 : 0.95 : 0.05 to the basic solution consisting of 35 mL of THAM 0.4 g L^{-1} and 5 mL NaOH 1 M under vigorous mixing (1000 RPM). After mixing for 30 minutes, the particles were washed before aging at 80 °C for 4 h in a Teflon reactor. After reaching room temperature, the particles were dialyzed (6–8 k MWCO dialysis tubing, Thermo Fisher Scientific) against water (35 mL/900 mL) for 3 cycles before characterization. For S-LDH multi-inlet vortex mixer (MIVM)[48] was used for the mixing stage while all other procedures stayed the same. In all cases specified, LDH preserved the size stability for at least one month after preparation due to its small size and high ZP.

Tb release from the LDH surface. L-LDH solution was diluted with either DI water or simulated apo-plastic fluid (SAF), pH 5.5 at a 1 : 2 volume ratio. After 24 h the solution was transferred to an Amicron filter (MWCO of 10 kDa) and centrifuged. The filtrate concentration of Tb in the filtrate was measured by ICP-MS after digestion, and Tb release from the LDH surface was compared to the ability of Tb salt, at the same concentration, to pass through the filter.

LDH modification by ssDNA-Cy3. ssDNA-Cy3 in the range of 0.02–0.08 g L^{-1} was added to S-LDH (0.7 g L^{-1}) and mixed thoroughly. The adsorption was quantified upon centrifugation by measuring the fluorescence level (using a plate reader, Tecan Spark) of the supernatant against the calibration curve of ssDNA-Cy3. Upon modification, the size and ZP were measured by DLS as specified below. S-LDH and L-LDH modified with Cy3 were produced using L S^{-1}-LDH (0.7 g L^{-1})-ssDNA-Cy3 (0.04 g L^{-1}) and then diluted to 0.5 g L^{-1} before application. The fluorescent shift was monitored on the suspension of these particles.

LDH characterization

LDH (for both versions) size, polydispersity index, and ZP were measured using a Malvern Zetasizer Nano (Malvern Instruments). LDH was diluted tenfold in DI water before size measurement and ZP measurement (NaCl 0.5 mM pH 8), measurements were performed in triplicate. For TEM, 4 μL of the LDH suspension was added to a TEM grid (Carbon Type B on 200 mesh thick grid), and the solution was evaporated overnight before imaging by FEI Tecnai F20 TEM at an acceleration voltage of 200 kV (resolution, 2048 × 2048 pixels; CCD camera, Gatan Rio). The metal content of the LDH and accordingly the total concentration was quantified by inductively coupled plasma mass spectrometry (ICP-MS). To 0.1 mL of LDH suspension, 0.5 mL of nitric acid (70%) was added. After 3–4 h digestion, appropriate dilutions with DI water were made, and the solution was filtered through an H-PTFE filter of 0.45 μm. The metal content of the samples was then measured using an Agilent 7700 ICP-MS. Dissolved ^{25}Mg, ^{27}Al, and ^{159}Tb concentrations were recorded in triplicate in 'no gas' mode. LDH were centrifuged at 17 000*g* for 1 h and were lyophilized before being characterized by Malvern Panalytical Empyrean XRD and Fourier-transform infrared (FTIR) Shimadzu (8400 s, Japan). S-LDH was characterized using inductively coupled plasma (ICP) time-of-flight (TOF) mass spectrometry operated in single-particle mode. The method was able to detect individual or aggregated individual particles using TOFWERK (CH) icpTOF R ICP-TOF-MS. Briefly, samples were introduced into the plasma by using a perfluoro alkoxy alkane (PFA) self-aspirating nebulizer with a measured flow rate of 54 μL min^{-1}. The nebulizer was inserted into a linear PFA flow chamber, connected to a 1.8 mm sapphire injector, and nickel cones were used.[49] Samples and dissolved standards were recorded for 10 and 1 min, respectively. Dissolved standards included the isotopes ^{24}Mg, ^{27}Al, ^{159}Tb, and ^{197}Au between 0.1 and 20 ppb. 40 nm gold (Au) NP (NanoXact, Nanocomposix) were used as a size standard to determine the transport efficiency.[50] Particle events, recorded with a 2 ms dwell time, were separated from the dissolve background if larger $\mu + 3.29\sigma + 2.72$ (μ and σ are the average and standard deviation of the instrument signal, respectively)[51] implemented in the instrument software code. The particle data was exported for further processing in Origin (Software).

LDH -plants interactions

Tomato growth. Tomato plants (Solanum Lycopersicon, Roma VF) were grown hydroponically in quarter-strength Hoagland's solution. Tomato seeds were rinsed in 10% bleach for 1 min and then rinsed in DI water 5 times. The sterilized seeds were germinated on water-moistened filter paper in a Petri dish for 8 days in the dark. The seedlings were then transplanted to 100 mL plastic cups. Plants were grown individually at 22 °C with a 16 h light and 8 h dark cycle for 3–4 weeks before LDH foliar exposure.

Foliar LDH dosing on tomato plants. Foliar LDH dosing on tomato plants- The LDH solution was pipetted onto the leaf's center (the tip was in loose contact with the leaf surface, Fig. S1†), moving over the leaf to get a homogeneous coverage. For adaxial application, the leaf was held horizontally to prevent the solution from dripping off until the NC solution was fully distributed across the leaf. For abaxial application, the leaf was turned over, and the solution was pipetted onto the leaf in the same manner (Fig. S1†). When we applied the solution more than once to the same leaf, we waited until the leaf was dry before applying the next dose. Silwet L-77 0.05% v/v was used to promote spreading and complete coverage; no visible leaf damage was observed at this Silwet concentration (tested from both sides of the leaves). The leaves were numbered from bottom to top (#1 for the older and lower leaf, *etc.*, not including cotyledons). This procedure was chosen to prevent any loss of particles during application, improving the reproducibility of the results.

Leaf attachment. This procedure was done based on Shen *et al.*, 2020 (ref. 52) with modifications. 20 μL of L-LDH doped with 13 ppm of Tb was deposited on the 3rd and 4th real leaves of tomato using a pipette in the presence of Silwet L-77 (0.1% v/v). L-LDH was applied from the adaxial and abaxial sides of the leaf and as a control Tb salt was applied in the same concentrations and conditions. 24 h after application, leaves were cut off the plants and washed in 50 mL tubes with 15 mL of DI water; the leaves were shaken in the solution for 1 min. Then, leaves were dried for 48 h at 80 °C. The wash solution and the leaves were digested either by Nitric acid 70% (wash solution) or by Nitric acid 70%: hydrogen peroxide 30% at 2:1 ratio (leaves). For the leaves, an additional stage of heating the digestion solution under 90 °C for 1 h was added. After suitable dilution, Tb concentration was measured in both washing solution and leaves digestive solution by ICP-MS to monitor Tb concentration. For each treatment, 4 repetitions were taken.

Stomata density. The stomata density was measured by peeling the cuticle from both sides of the leaves according to.[53] Stomata were counted under a light microscope with 40× magnification, and 5 repetitions for both abaxial and adaxial sides were taken.

Uptake pathway by confocal microscopy. The uptake routes of S-LDH into the leaf were tracked by confocal fluorescent microscopy (Zeiss 880) using Cy3-modified S-LDH. For adaxial and abaxial applications 50 μL of S-LDH-Cy3 (0.5 g L^{-1}) were applied on the 3rd or 4th leaf of a 3- to 4-week-old tomato plant 20 h before imaging. S-LDH-Cy3 was supplemented with 0.05% v/v for adaxial or abaxial sides. Before imaging the leaf was gently washed with DI water to remove unattached S-LDH from the surface. For getting fluorescence from the cuticle 50 μL of auramine O in HCl-THAM solution(1 g L^{-1}) pH 7.2 (ref. 54) with Silwet L-77 (0.05%) applied on the leaf just before the imaging.

The uptake routes of S-LDH-Cy3 in tomato leaves were imaged using a scanning confocal microscope with 40× objectives (EC plan-neofluar 1.3 oil DIC M27). A leaf section was cut, mounted on a glass slide, immersed with oil mounting media, and covered with a coverslip. Excitation wavelengths for auramine O, S-LDH-Cy3, and chlorophylls were at 458, 514, and 613 nm, respectively. Detection ranges were 491–540, 552–632, and 647–721, for auramine O, S-LDH-Cy3, and Chlorophylls, respectively. Each of the factors (S-LDH-red, Cuticle-blue, chloroplast-green) has a complete isolate excitation and emission range and in addition, subsequential excitation and emission cycles were used to avoid interference between the channels (Fig. S8†). As control samples, one leaf from both adaxial and abaxial sides (applied only with 0.05% v/v silwet L-77 in DI water) was imaged and the parameters were adjusted so no fluorescence of the auramine and Cy3 can be seen for the control. To get a complete description of S-LDH penetration through the leaf, *z*-stacking imaging was conducted (30–40 μm, resolution 1 μm, and ~50% overlapping between stacks). At least 3 repetitions were taken from each treatment. Confocal microscopy images were analyzed using Zein lite or FIJI (ImageJ).

S-LDH coverage on the leaf was calculated by z projection and color thresholding of S-LDH in comparison to the overall surface (based on 3 independent images) of the leaf using ImageJ. The same procedure was applied for stomata coverage with the overall aperture area of the stomata measured by the auramine O channel.

Mander coefficients were obtained based on the z-profiles of the *z*-stacks (orthogonal view) by ImageJ using the JACoP plugin. Since auramine O was also able to enter through the stomata, profiles of only the cuticle were taken for this analysis.

Imaris analysis. Sections of AbC, AdC, and AbS with the same size were selected, and S-LDH, cuticle, and chlorophyll channels were represented as surfaces. For mesophyll and cuticle main setup factors were smoothing with 1 μm surface grain size and growing estimated diameter of 2 μm. For a better representation of the surfaces, we used filtering by quality for the mesophyll and filtering by Z height for the cuticle. The penetration of auramine O through the stomata was corrected by creating a representative surface of its penetration pattern. Accordingly, that surface was masked out from the cuticle surface. For S-LDH no smoothing was used, growing estimated diameter of 0.5 μm was defined, and filtering was applied by the quality values. To avoid misinterpretation, S-LDH NP which were found on the outer cuticle were removed for analyzing the ratio of overlapped volume and the shortest distance to the cuticle, (found only for the abaxial side).

LDH application without nutrition deficiency

S-LDH was dosed foliarly on 4-weeks-old Roma tomato seedlings grown hydroponically in quarter-strength Hoagland's hydroponic solution (all nutrients available). Four subsequential applications of 200 μL were applied every 3 days. Each application (200 μL) was done by pipetting 20 μL of S-LDH on real leaves 3–6 until the whole volume was used. On the abaxial

side, S-LDH at 0.05–0.3 g L^{-1} was applied and on the adaxial side 0.15 g L^{-1} was applied as a comparison to the abaxial application (4/5 plants per treatment); in all cases, Silwet L-77 0.05% v/v was added to the solution. For control plants, DI water + 0.05% Silwet L-77 was applied on the leaves. 10 days after the last application, the CO_2 assimilation of the applied leaves (leaf #5) was recorded as a function of the light intensity using Li-Cor Li-6800 (plants were light-equilibrated before measurement) following[55] with modifications. Light response curves were measured at T = 30 ° C, RH = 60% Ci = 400 ppm and were acquired at 1500, 1200, 900, 600, 400, 300, 200, 100, 50, and 0 μmol m^{-2} s^{-1}.

LDH application under Mg deficiency

4-week-old Roma tomato seedlings were grown hydroponically in complete quarter-strength Hoagland's hydroponic solution. After 4 weeks the plants were transplanted to quarter-strength Hoagland's solution under Mg deficiency ($NaSO_3$ instead of $MgSO_3$) for 5 days before initial application of S-LDH. 4 successive applications (every 1 or 2 days) of S-LDH in 10 mM MES buffer solution pH 6.1 (ref. 30) at 2.5 g L^{-1} was abaxially or adaxially applied on real leaves 3–6 in the presence of Silwet L-77 0.05% v/v. The size of S-LDH was tested in the buffer solution by DLS and no change in size was observed (Table S7†). The overall volume applied was 1.5 mL divided between the applications; as a control, plants without any application were used. Plants were harvested 2 weeks after the beginning of starvation and were divided into 3 sections: roots, main shoot, and unexposed leaves. Plant sections were dried at 80 °C for 72 h and then weighed. Roots and shoot tips were digested based on.[10] Two mL of 2 : 1 mixture of nitric acid 70% and hydrogen peroxide 30% for 24 h and then heated to 95 °C for 1 h before dilutions and measured by ICP-MS, (Mg, Tb, Zn, Mn, Fe, Cu were monitored). Each treatment had 5 replicates.

Results and discussion

LDH synthesis and characterization

Two versions of LDH with different sizes were synthesized: large LDH (L-LDH) and small LDH (S-LDH). The dynamic light scattering (DLS) number size of the L-LDH was 53 ± 9 nm and the PDI was 0.19 while the DLS number size of the S-LDH was 37 ± 1.5 nm ($p < 0.04$) and the PDI was 0.13 (Fig. 1a and Table S1†). The LDH crystal structure was confirmed using X-ray powder diffraction (XRD) and attenuated total reflection Fourier transform infrared spectroscopy (ATR-FTIR) analysis (Fig. 1b, Table S2, and Fig. S2† for detailed analysis). Transmission electron microscopy (TEM) images indicate the formation of LDH with rounded to hexagonal shape with a statistically different average size of 57 ± 20 nm for L-LDH and 44 ± 13 nm for S-LDH ($P < 0.0001$) (Fig. 1c and d, and Table S3†). The trends in both measurement methodologies (DLS and TEM) were similar, with smaller and more homogenous particles formed when using the MIV mixer. Zeta potential (ZP) measured in 0.5 mM NaCl at pH 8 resulted with +36.6 ± 0.2 and +38.6 ± 1.0 mV for L-LDH and S-LDH, respectively.

The LDH particles were doped with terbium (Tb) (5% of aluminum (Al) molar concentration) (Fig. 1e and S3†) as a tracer metal to quantify the particles' association with the leaves upon foliar application and to monitor their distribution in the plant tissues. The ratio of Mg/(Al + Tb) was 2.67 ± 0.07 and 3.33 ± 0.03 for S-LDH and L-LDH, respectively with similar Tb/Al ratio (0.049 ± 0.001 and 0.053 ± 0.002, respectively). A single particle inductively coupled plasma time-of-flight mass spectrometry (ICP-TOF-MS) measurement was conducted to determine the metal composition of hundreds of individual particles in the population and compared to the bulk chemical data measured by ICP-MS of acid-digested particles (Fig. 1e and S2†). While the molar ratio of Tb/(Mg + Al + Tb) in the particles was mostly in the range of 1–2%, (Fig. 1e), the ratio between Mg and Al ranges between 57–95% for Mg and accordingly 42–4% for Al. However, the majority of the particles represent a ratio close to the values obtained by the ICP-MS (Fig. 1e and S2†) indicating that the Tb is relatively uniformly distributed in the S-LDH particles. The Tb in the structure was not leached from particles dispersed in deionized (DI) water or stimulated apo-plastic fluid (SAF) after 1 day (Table S4†). Since the Tb ratio in particles is relatively constant and the Tb does not leach out, it is a reliable indicator of the presence of LDH.

Attachment and internalization pathways of foliarly applied LDH

Rain-fastness is an important agrochemical property that encapsulation into NC is expected to improve,[9] so the L-LDH attachment with the leaves after foliar application to either side of the leaves was measured. As a control, $TbCl_3{\cdot}6H_2O$ at the same concentration was applied to separate plants. The leaf-associated Tb was quantified 24 h after application following a washing step. Tb was also quantified in the washing solution to close the Tb mass balance (Table S5†). The association of L-LDH to the leaf surface from both sides of the leaf was substantially higher in comparison to the salt (Fig. 3a); 84.5 ± 17.3% and 76.2 ± 12.8% for L-LDH in comparison to 28 ± 6.3% and 35.8 ± 10.9% for Tb salt from the adaxial and abaxial side, respectively. The higher association can evolve from the layer structure producing a higher surface area that in combination with the positively charged surface promotes strong interactions with the acid functional groups in the cuticle.[56] While there is a similar attachment between L-LDH on both sides of the leaf, the distribution and uptake into the plant differed in several important ways as described below.

To assess the distribution of LDH on leaf surfaces the S-LDH particles were tagged with 15 base single-strand DNA-Cy3 (ssDNA-Cy3) to form a stable suspension of S-LDH-Cy3 complexes. The adsorption of ssDNA-Cy3 to the surface was 90% when added at 0.04 g L^{-1} and the release was negligible (Table S6†). The adsorption of ssDNA-Cy3 was verified by

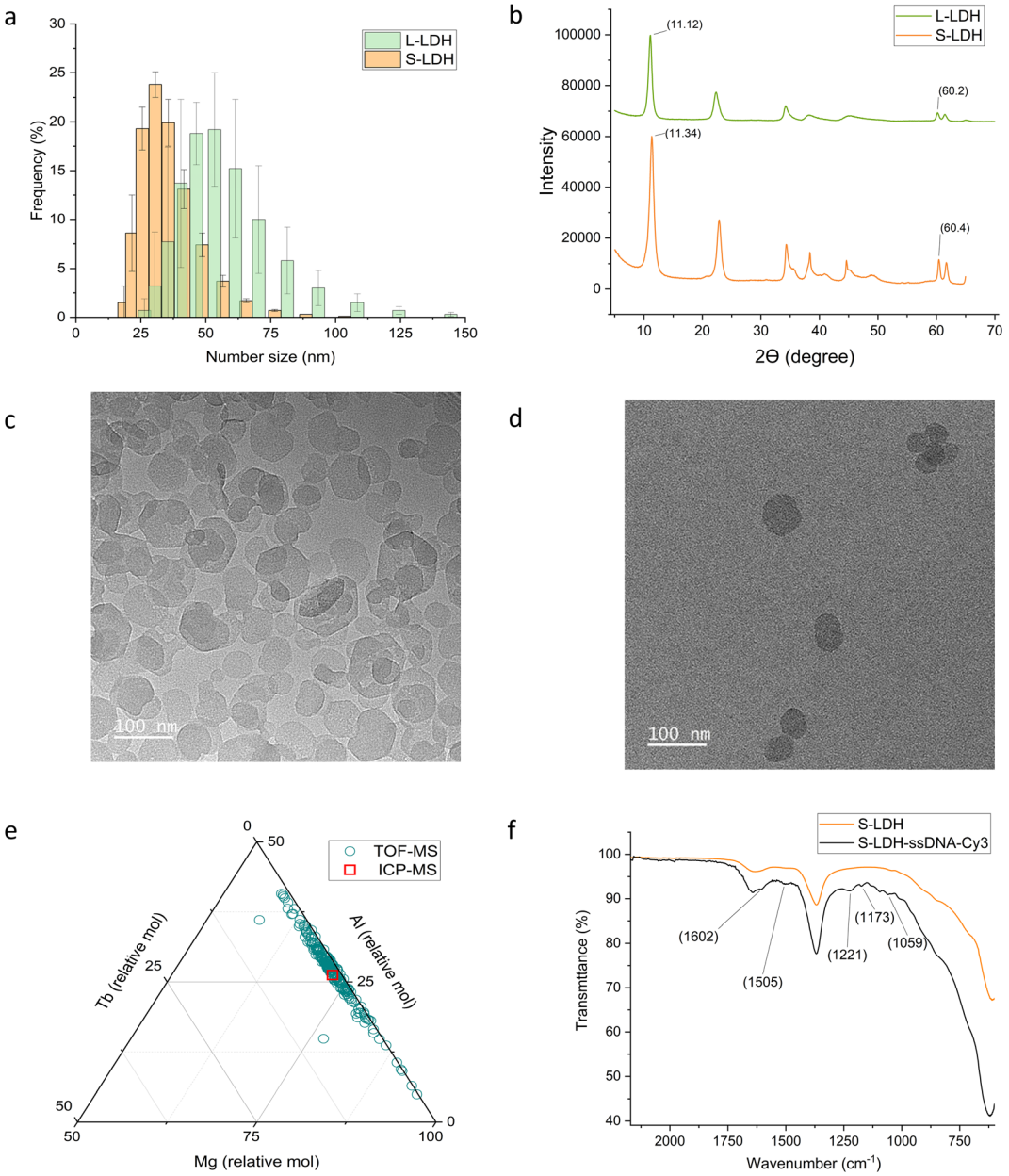

Fig. 1 S-LDH and L-LDH characterization and surface modification. (a) Size distribution by DLS measurements. (b) XRD spectra. TEM images of (c) L-LDH and (d) S-LDH. (e) Metal ratio description of S-LDH obtained by single particle ICP-TOF-MS. The red square represents the value obtained by ICP-MS. (f) ATR spectrum of S-LDH-ssDNA-Cy3 in comparison to the S-LDH.

ATR-FTIR measurements (Fig. 1f and S4†), and by the change in the Cy3 fluorescence pattern upon adsorption (Fig. S5†). By ATR-FTIR, among other peaks that appeared between 1650–1000 cm^{-1} upon adsorption, the most direct evidence for ssDNA-Cy3 adsorption is the peak at 1221 cm^{-1} which is assigned to the nucleotide's PO_2^- stretching.[57,58] Upon tagging with ssDNA, the number size of S-LDH was increased by ~20 nm while the zeta potential stayed highly positive (Table S7†) promoting stability against aggregation. S-LDH was applied to leaves in water amended with Silwet L-77 (0.05% v/v) and confocal images were taken 20 h after application (Fig. 2b, 3a, and b).

The distribution of S-LDH on the leaf's surfaces (stomata and cuticle) was monitored on both the adaxial and abaxial sides (Fig. 2b). The abaxial side had a high stomata density (~160 stomata per mm^2), while the adaxial side had an almost negligible stomata density (~3 stomata per mm^2) (Table S8 and Fig. S6†). By measuring the average area of the stomata opening, we found that the abaxial side of the leaf, with a high density of stomata, accounts for only 0.74 ± 0.22% of the leaf surface area and negligible coverage for the adaxial side (0.011 ± 0.02%) (Table S8†). Accordingly, we followed the coverage of S-LDH on the leaf surfaces using confocal microscopy. On both sides of the leaf, S-LDH

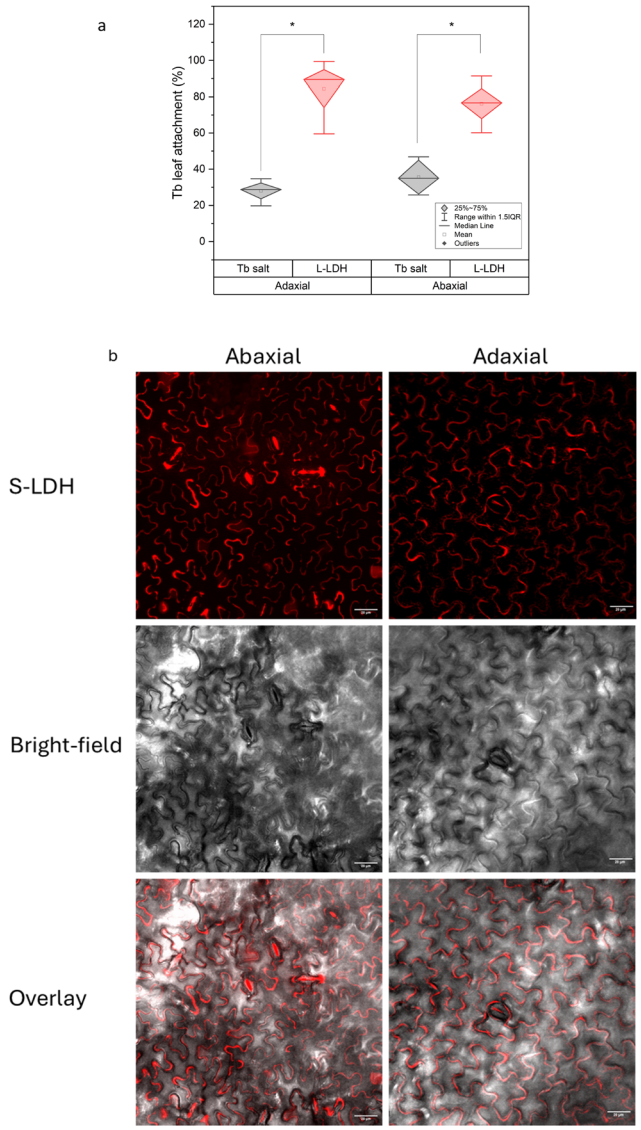

Fig. 2 Attachment of LDH with tomato abaxial and adaxial leaf surfaces. (a) Comparison between L-LDH and Tb^{3+} salt applied from either abaxial or adaxial sides. Statistical analysis was done using one-way ANOVA followed by Tukey test, significance level for * $p < 0.01$, $n = 4$. (b) S-LDH distribution on leaf surface from adaxial and abaxial sides obtained by confocal microscopy.

coverage on the cuticle was similar (11 ± 2% and 10 ± 1% of the leaf surface area for the adaxial and adaxial sides, respectively) (Fig. 2b). For both sides, S-LDH was found concentrated in the outlines of the epidermal cells. That pattern may result from using Silwet L-77 which promotes spreading to these intercellular regions of the leaf epidermis. For the abaxial side, the localization of S-LDH in stomata 20 h after application was evaluated. We found that for the abaxial side, 58 ± 20% of the stomata area was covered with S-LDH, and in addition, 63 ± 22% of the stomata were found partially or fully colocalized with S-LDH. The colocalization of S-LDH with the stomata was measured by its distribution in both the horizontal (XY plane) and vertical (z-profile) in comparison to the cuticle (Fig. S7†). The presence of S-LDH in the stomata pores suggests the ability of S-LDH to enter through these micron-sized epidermal pores and the potential for S-LDH to interfere with the stomata function. There was a higher probability of locating S-LDH beneath the cuticle (Fig. 3a, lower panel) for leaf sections that included stomata compared to leaf sections without stomata. We further investigated how the observed uptake pathways affect S-LDH penetration into the leaf.

To better track the penetration of S-LDH into the leaf from both sides, *z*-stacks of the leaves were obtained while the fluorescence of the cuticle, S-LDH, and the chloroplast was monitored (cuticle-blue, S-LDH-red, chloroplast/mesophyll-green; for control images of cuticle and LDH alone, see Fig. S8†). For S-LDH applied on the abaxial side, the particles are primarily associated with the cuticle layer (marked by auramine O, Silwet L-77 0.05% v/v) and there was limited penetration of the particles into the leaf (Fig. 3a upper). In contrast, for adaxial application, S-LDH penetrates through the cuticle into deeper parts of the leaf (Fig. 3b and S9†).

To quantify these differences in cuticle association and leaf penetration, Mander's colocalization coefficient was used to measure the intensity of colocalization of S-LDH within the cuticle. These measurements were based on the profiles of the fluorescence signals along the *z*-axis (orthogonal images). The Mander's colocalization coefficient for the abaxial and adaxial applications were 0.41 ± 0.04 and 0.18 ± 0.05, respectively (Fig. S10†). These cuticle colocalization results demonstrate that when applied abaxially, the association with the cuticle is higher while when applied adaxially, S-LDH penetrates to a higher extent into the leaves and the epidermis layer. When looking at abaxial sections that include stomata (Fig. 3a, lower panel), S-LDH can be found completely detached from the cuticle and in the inner parts of the leaf (white arrow) demonstrating that despite the relatively low coverage of stomata on the leaf surface (Table S8†), it is a main penetration route. The stomata uptake route is not expected to be substantial for the adaxial application.

To better understand the S-LDH penetration patterns and to analyze the trends on a more extensive surface area of the leaf, we define the distribution of S-LDH, cuticle, and chloroplasts at the *z*-axis through their respective fluorescence signals in a 3D volume rendering (Imaris software, surface modeling). By inspecting 3 application regions of the leaf area (adaxial-cuticle (AdC), abaxial cuticle (AbC), and abaxial stomata (AbS)) it is possible to evaluate the contribution of each of the sections to the S-LDH uptake into the leaves. The average penetration gap between S-LDH and the cuticle was 2.47 ± 0.07, 1.25 ± 0.13, and 0.75 ± 0.1 μm for the AdC, AbS, and AbC, respectively (Fig. S11†). Additional parameters describing S-LDH penetration include the ratio of the overlapped volume of the S-LDH fluorescence signal with the cuticle signal (Fig. 3c) and the shortest distance from the cuticle (Fig. 3d). S-LDH applied on the adaxial side (AdC) had 13% of the particles with low overlapped volume (defined as <50% of the particle volume colocalized with the cuticle) compared to only 3% of the

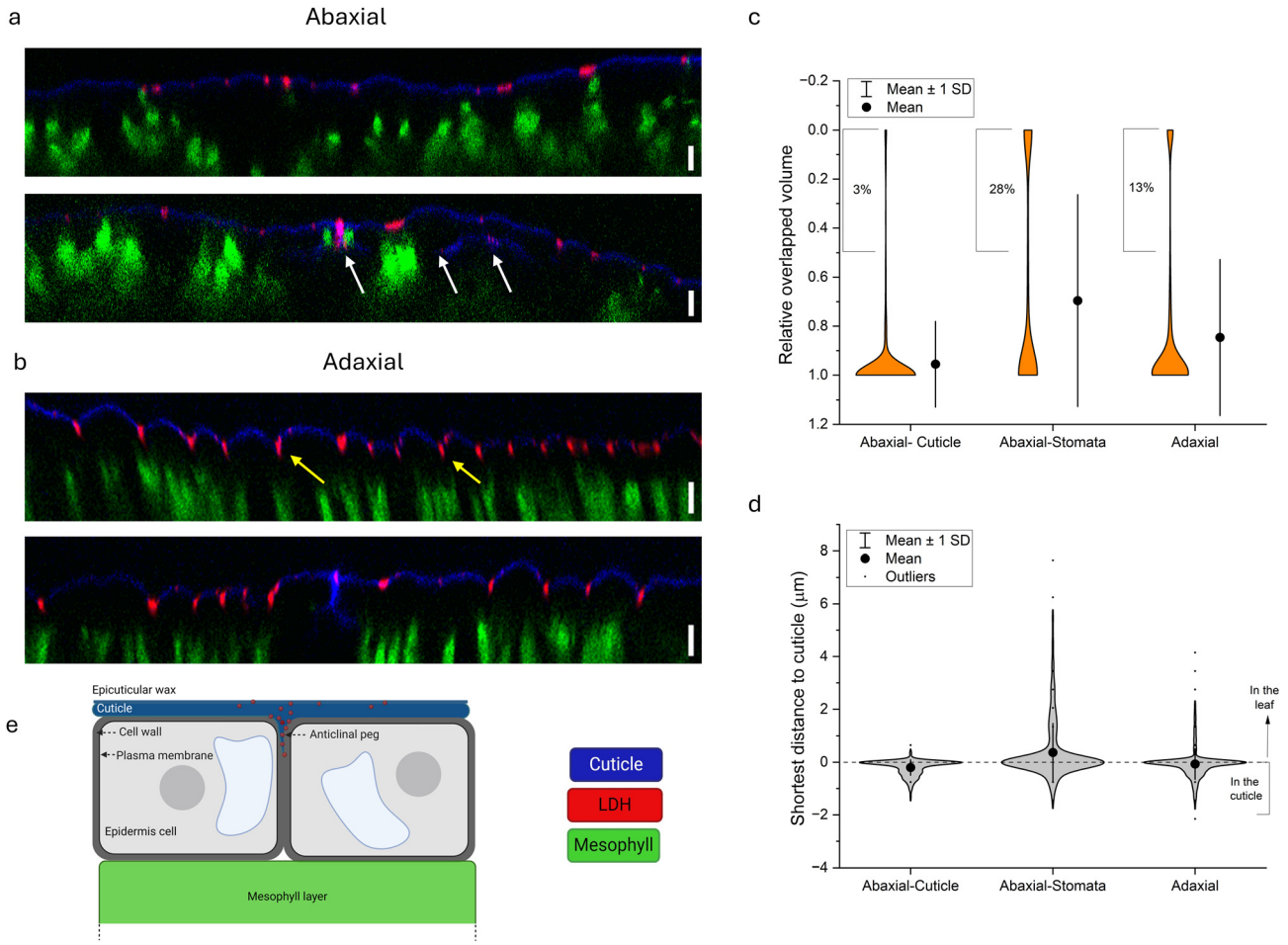

Fig. 3 LDH internalization pathways into tomato leaf. (a and b) Orthogonal display of the z-stack imaging by confocal microscopy, blue, red, and green represent the cuticle, S-LDH, and chloroplast, respectively. (a) Abaxial application- cuticle section (upper) and stomata section (lower, white arrow points to S-LDH that internalized through the stomata). (b) Adaxial application-cuticle section (upper, yellow arrows point to the anticlinal pegs) and stomata section (lower), scale bar = 10 μm. (c and d) Parameters describe the localization of S-LDH in relation to the cuticle as obtained by 3D volume rendering. (c) The distribution of the relative overlapped volume of S-LDH particles within the cuticle (ratio of 0–0.5 related to particles located mostly below the cuticle). (d) The distribution of the shortest distance of S-LDH particles in relation to the cuticle (negative to zero values represent particles embedded in the cuticle, while positive values represent the penetration depth compared to the cuticle). (e) An illustration of S-LDH penetration through the cuticle of the adaxial side and accumulation in the anticlinal pegs as suggested by the confocal images.

S-LDH in the case of the abaxial application (Fig. 3c). That greater amount of S-LDH with lower overlapped volume indicates that S-LDH more easily penetrated through the cuticle into the inner parts of the leaf when applied from the adaxial side (top) compared to the abaxial side (bottom). For AbS, 28% of the NP showed low overlapped volume (Fig. 3c) emphasizing the significance of uptake through stomata into deeper parts of the leaf. The distribution of S-LDH-cuticle shortest distance also demonstrates that the particles that penetrated through the stomata were able to move further into the leaf with maximum values of 0.8, 4.2, and 7.7 μm for AbC, AdC, and AbS, respectively (Fig. 3d). Overall, the results indicate that both cuticular uptake and stomata uptake routes are possible. For cuticular uptake, S-LDH penetrates through the cuticle to a higher extent and moves into deeper layers of the leaf when applied adaxially compared to abaxially. However, stomata uptake on the abaxial side provides the deepest penetration into the leaves compared to the other uptake routes. While the uptake through the stomata has been suggested as a main pathway for NC uptake,[59] cuticular uptake, especially through the adaxial side, appears also to be significant.

The observed S-LDH penetration pattern from the adaxial side is consistent with the structure of the cuticle. Heredia-Guerrero *et al.*, 2014 (ref. 36) provided an in-depth characterization of the cuticle. The cuticle penetrates between two adjacent epidermis cells to form the anticlinal peg. This extended cuticle in this region comprises different components (from top to bottom): wax, cutin, intracuticular waxes, phenolic compounds embedded in the cutin, and a layer of polysaccharides at the proximity of the cell wall.[36] The penetration pattern observed by the confocal images suggests that the S-LDH NP diffuse through the cuticle, are directed to the anticlinal pegs, and travel through them toward the cell wall

(Fig. 3e). However, because of the size limitation of the cell wall (known to be <20 nm with some evidence for exceptions[60]), S-LDH appears to get trapped in this location.[61] The ability to direct NC to the anticlinal pegs can be used to deliver an active agent even without penetrating the cell wall,[62] and potentially improve the plant's resilience toward biotic stress. For example, botrytis cinerea penetrates through anticlinal pegs in its way to internalize the cells.[63] The ability of the S-LDH to diffuse into the anticlinal pegs and accumulate there can be used to fortify cuticle resistance against biotic invaders; either as a carrier for active ingredients (*i.e.* anti-fungal molecule) or by doping an active component such as Cu into the LDH structure.[64] The improved rain-fastness and the high coverage of LDH on the cuticle at the epidermal cells' outline and the ability to diffuse into the cuticle-cell wall interface can be used for a sustained release of AA molecules with systemic mobility.

Although delivery through the cuticle is an important pathway due to the high surface area of the cuticle on the leaves compared to stomata, the delivery of NC through stomata is highly desirable since it provides a direct pathway to the mesophyll. The extent and the efficiency of stomatal entry may depend on many parameters, including the environmental conditions and the physiological state of the plant as these affect the opening of stomata.[65,66] In addition, the presence of an adjuvant in the delivery solution since it can promote stomata flooding.[67] However, the entrance of NC through the stomata might pose physical constraints on the plant. That was implied by the colocalization of S-LDH on the stomata as measured 20 h after application. As previously reported, silica NC were observed clogging the stoma aperture, disrupting its functionality.[33] Depending on the extent, this phenomenon can potentially interfere with leaf gas exchange or other plant

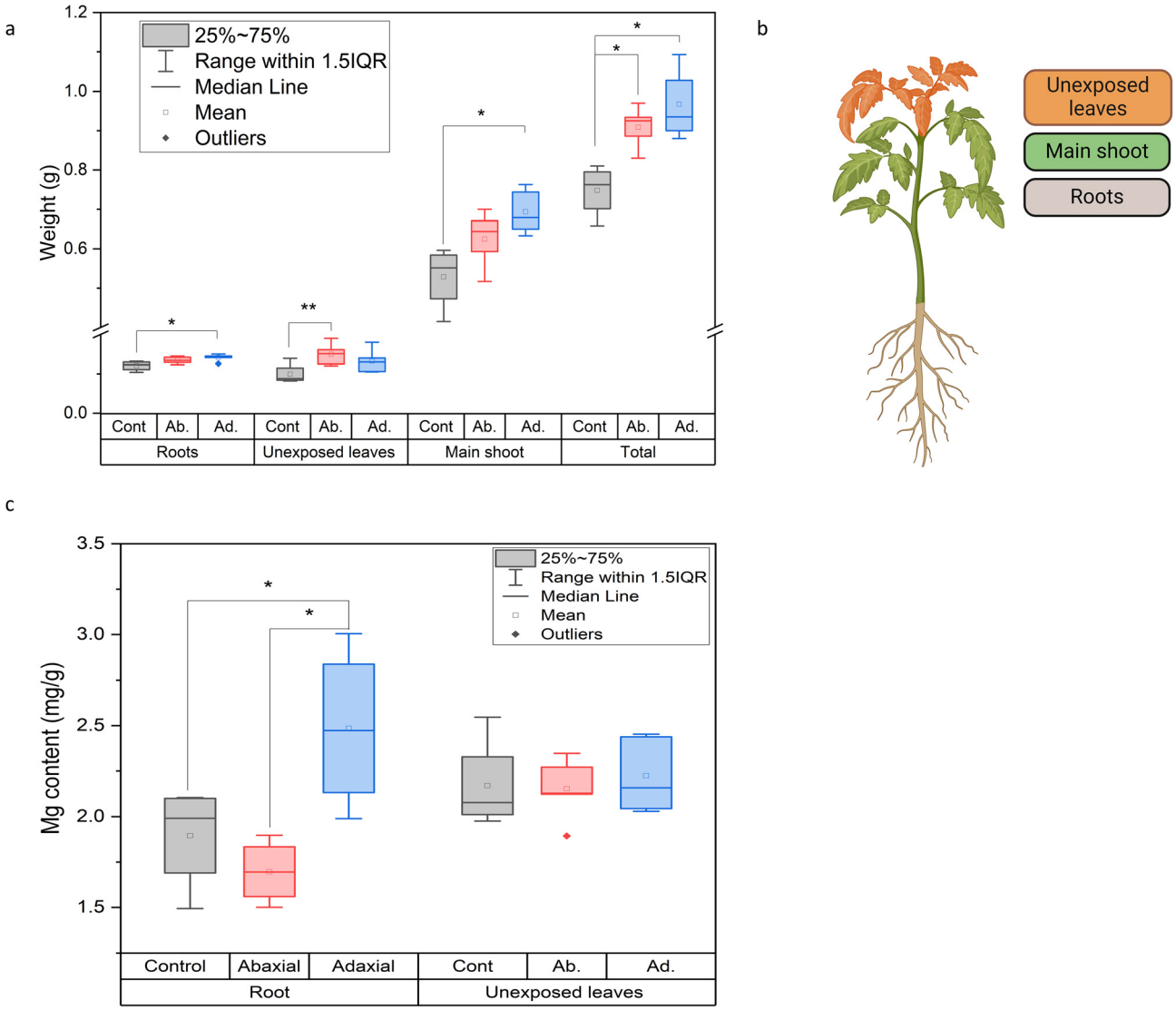

Fig. 4 Effect of adaxial and abaxial applications of S-LDH (2.5 g L^{-1}) on (a) weight accumulation. (b) An illustration of the plant sections that were tested. (c) Mg concentration in selected organs under conditions of Mg deficiency. Statistical analysis for graphs a and c was done using one-way ANOVA followed by the Tukey test. For graph a, significance level for * $p < 0.05$, and ** $p < 0.1$, $n = 5$. For graph c, * $p < 0.07$, $n = 5$.

physiological processes. Based on the differences observed between leaf uptake pathways for S-LDH, we studied how foliar delivery pathways of S-LDH affect Mg delivery and plant performance.

LDH foliar delivery pathway effects on plant growth and physiology

The effect of the different leaf uptake pathways of S-LDH on plant growth and nutrient delivery was evaluated. To test the contribution of Mg from S-LDH, plants were grown under Mg deficiency (1/4 Hoagland solution without Mg) and S-LDH was applied foliarly. The plant dry weights (Fig. 4a) of the main shoot (on which S-LDH was applied), unexposed leaves, and roots were measured (Fig. 4b). Adaxial and abaxial applications displayed 29 ± 17% and 21 ± 13% higher weight gain for the whole plant in comparison to the control (no addition of Mg). Adaxial application showed statistically significantly higher weight gain for both the main shoot and the roots (31 ± 23% and 17 ± 14% respectively) compared to the control plants (Table S9†).

The Mg content in the unexposed leaves and roots was measured by ICP-MS to evaluate the ability of the S-LDH applied on the leaves to provide Mg to other plant organs (Fig. 4b and c). For the shoot tip, no difference was observed in terms of mg Mg g^{-1} dry weight. This is likely because plants prioritize nutrient transport to the actively growing parts over the more established ones.[68] However, the adaxial S-LDH treatment displayed a substantially higher concentration of Mg in the roots in comparison to both the control and abaxial application, indicating that the adaxial application provided better long-distance delivery of Mg. The absence of Tb in the roots indicates that the translocation mechanism relies on the dissolution of the S-LDH in the leaves and subsequent translocation of dissolved Mg in the plant rather than translocation as an S-LDH NP.[69] We hypothesize that the proximity of the S-LDH to the epidermis cell wall may expose it to a lower pH (~5.5–6) at the cell wall surfaces,[25,26] promoting LDH dissolution and release of dissolved Mg. The data suggests that adaxial application can better deliver nutrients to the plant as demonstrated by the higher weight gain and better translocation of Mg to the roots. However, the availability of Mg from S-LDH is only partly responsible for the increased growth relative to controls as the abaxial application did not show better translocation of Mg but did improve growth. To study

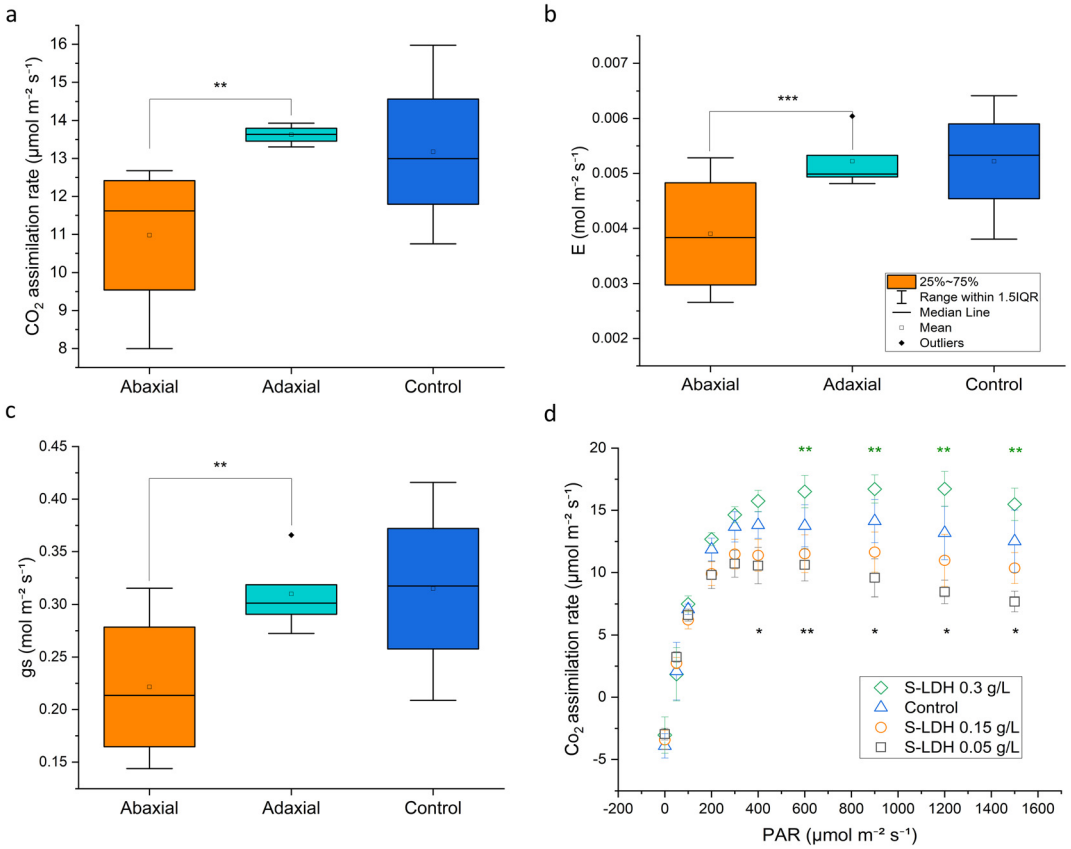

Fig. 5 Effect of S-LDH application on leaf gas exchange and photosynthesis parameters. (a) Carbon dioxide assimilation rate, (b) transpiration rate, (c) and stomatal conductance compared between adaxial and abaxial application of S-LDH at 0.15 g L^{-1}, light intensity of 1200 μmol m^{-2} s^{-1} (d) CO_2 assimilation rate as a function of light intensity (PAR) and S-LDH concentration, application from the abaxial side. Statistical analysis was done using a t-test for graph a–c and using one-way ANOVA followed by the Fisher LSD test for graph d (comparison to the control). Significance level for * $p < 0.01$, ** $p < 0.05$ *** $p < 0.07$, $n = 4$ or 5, and errors represent SD.

additional effects promoted by LDH, different leaf physiological parameters upon foliar application were measured.

Application of S-LDH to the adaxial side of the leaf had no effect on plant physiology, whereas application to the abaxial side showed some inhibitory effects. S-LDH was applied at 0.15 g L^{-1} on either the adaxial or abaxial sides of the leaves and the effect on different parameters related to leaf gas exchange and photosynthesis were measured (using 1/4 Hoagland solution, no Mg deficiency). Stomata conductance (gs), transpiration rate (E), and CO_2 assimilation rate (A) showed higher values for the adaxial treatment compared to the abaxial treatment (Fig. 5a–c and S12†). The lower values of gs (0.22 *vs.* 0.31 mol m^{-2} s^{-1}) and E (0.0039 *vs.* 0.0052 mol m^{-2} s^{-1}) for abaxial application suggest that S-LDH interferes with the stomata functionality,[33,70] which is supported by confocal imaging showing the presence of S-LDH in the stomata pores (Fig. S7 and Table S8†) which in turn, inhibits CO_2 assimilation (11.5 *vs.* 14.34 μmol m^{-2} s^{-1}). The same trend was also evident in photosystem II quantum yield (ΦPS2) levels (0.095 *vs.* 0.114), (Fig. S13†), indicating that the light reactions of photosynthesis were also impaired by the abaxial application. In contrast, the adaxial application and the control (Silwet L-77, 0.05% in DI water, 1/4 Hoagland solution), showed similar values at a concentration of 0.15 g L^{-1} (Fig. 5a–c). Surprisingly, the CO_2 assimilation rate demonstrated a concentration-dependent response where lower concentrations of S-LDH (0.05 g L^{-1}) showed the lowest A, and applying a higher concentration of S-LDH (0.3 g L^{-1}) enhanced the assimilation (Fig. 5d), (tested on the abaxial side). These differences were observed under A saturating light intensity (>600 μmol m^{-2} s^{-1}), where CO_2 assimilation is limited by the carboxylation capacity.[71] ΦPS2 and gas exchange parameters (gs, E,) followed the same trend (Fig. S14†), suggesting that S-LDH can have both suppressive and promotive effects on tomato leaf CO_2 assimilation,[72] and the final impact on the plant combines both effects. The promotive effect can be attributed to the higher availability of Mg, a key component of the photosystem chlorophyll porphyrin ring as was expressed by the ΦPS2 values (Fig. S13†). At the higher dose, S-LDH delivered more Mg and compensated for the inhibitory effect shown at the low concentration which was attributed to an impairment of the stomata's functionality. Altogether, the results indicate that S-LDH improved photosynthetic activity at higher concentrations of S-LDH while at lower concentrations the inhibition effect was predominant. In addition, the application from the adaxial side did not impair A while the abaxial application reduced it.

Conclusions

We determined LDH leaf attachment, uptake routes, and distribution in the leaf after foliar application from different sides of the leaves. LDH attachment to both abaxial and adaxial leaf surfaces was similar despite chemical and structural differences between these surfaces enabling improved rain fastness. From both sides, LDH covers 10–11% of the leaf surfaces concentrated mostly at the outlines of the epidermal cells. On the abaxial side, LDH was observed in stomata pores, potentially impairing leaf gas exchange and photosynthesis.

We followed internal distribution and penetration levels through 3 representative uptake pathways: adaxial cuticle, abaxial cuticle, and area of the abaxial surface with high stomata abundance. LDH penetrated through the leaf cuticle to a higher extent when applied adaxially compared to abaxially, and adaxial application has approximately twice as many particles with low association with the cuticle compared to abaxial application. LDH penetrated the deepest into the leaf when entering through the stomata and had the lowest association with the cuticle. For adaxial application, LDH were located within the anticlinal pegs situated between two adjacent epidermal cells. This proximity to the cell walls may facilitate a gradual Mg release mechanism in response to the expected lower pH near the cell wall. Based on these differences, a few aspects of plant health were evaluated. Under Mg deficiency, the adaxial application displayed higher weight gain in the roots, main shoot, and total weight. Furthermore, adaxial application showed enhanced Mg translocation to the roots demonstrating the ability of LDH to provide Mg to the plant through foliar application. These results were in line with leaf gas exchange and photosynthetic parameters that were found impaired in the abaxial compared to the adaxial application and the control.

Overall, we demonstrated that the LDH uptake pathways and the physiological response of the plant depend on the side of the leaf that they are applied to, *i.e.* the abaxial or adaxial sides. While the presence of stomata on the abaxial side of the leaf can improve the delivery of active agents into deeper layers of the leaf, LDH interferes with stomatal functionality, and the overall negative effect on the plant's physiology can be detrimental. Penetration of LDH through the cuticle on the abaxial side of the leaf was found to be limited. In contrast, applying LDH from the adaxial side which has a limited number of stomata, demonstrated several advantages: increased penetration through the cuticle compared to the abaxial side, higher mass gain, better Mg translocation to the roots, and enhanced photosynthetic activity. Since LDH is being used as a nanocarrier for applications in plant biotechnology and agricultural practices, this understanding of LDH-leaf interactions and the uptake mechanisms should promote improved utilization of LDH and other NC for more effective agrochemical practices.

Data availability

The data supporting this article has been included as part of the ESI.†

Author contributions

Hagay Kohay: writing – original draft, methodology, investigation, formal analysis, data curation, conceptualization, visualization, supervision, writing – review & editing, funding acquisition. Jonas

Wielinski: investigation, methodology, data curation, writing – review & editing. Jana Reiser: investigation, methodology, writing – review & editing. Perkins Lydia A: methodology, supervision, formal analysis, writing – review & editing. Kurt Ristroph: methodology, supervision, writing – review & editing. Juan Pablo Giraldo: funding acquisition, methodology, supervision, conceptualization, writing – review & editing. Gregory V. Lowry: funding acquisition, writing – review & editing, writing – original draft, methodology, supervision, visualization, conceptualization.

Conflicts of interest

There are no conflicts of interest to declare.

Acknowledgements

This research was supported in part by a Postdoctoral Award No. FI-599-2020 from BARD, The United States - Israel Binational Agricultural Research and Development Fund, and in part by a National Science Foundation (2133568) to GVL and JPG. J. W. acknowledges the Swiss National Science Foundation for supporting his work on this research project through the Postdoc Mobility program (Project no. P500PN_202844). The authors acknowledge the Materials Characterization Facility (MCF-677785) and Daniel Flaherty at Carnegie Mellon University for their guidance, support and for providing access to their instruments. Fig. 3e and 4b, and the graphical abstract were created using 'biorender'.

References

1 J. Hong, C. Wang, D. C. Wagner, J. L. Gardea-Torresdey, F. He and C. M. Rico, Foliar Application of Nanoparticles: Mechanisms of Absorption, Transfer, and Multiple Impacts, *Environ. Sci.: Nano*, 2021, **8**, 1196–1210, DOI: **10.1039/D0EN01129K**.

2 V. Takeshita, B. T. de Sousa, A. C. Preisler, L. B. Carvalho, A. do E. S. Pereira, V. L. Tornisielo, G. Dalazen, H. C. Oliveira and L. F. Fraceto, Foliar Absorption and Field Herbicidal Studies of Atrazine-Loaded Polymeric Nanoparticles, *J. Hazard. Mater.*, 2021, **418**, 126350, DOI: **10.1016/j.jhazmat.2021.126350**.

3 N. Mitter, E. A. Worrall, K. E. Robinson, P. Li, R. G. Jain, C. Taochy, S. J. Fletcher, B. J. Carroll, G. Q. Lu and Z. P. Xu, Clay Nanosheets for Topical Delivery of RNAi for Sustained Protection against Plant Viruses, *Nat. Plants*, 2017, **3**, 16207, DOI: **10.1038/nplants.2016.207**.

4 M. Zhu, J. Tang, T. Shi, X. Ma, Y. Wang, X. Wu, H. Li and R. Hua, Uptake, Translocation and Metabolism of Imidacloprid Loaded within Fluorescent Mesoporous Silica Nanoparticles in Tomato (Solanum Lycopersicum), *Ecotoxicol. Environ. Saf.*, 2022, **232**, 113243, DOI: **10.1016/j.ecoenv.2022.113243**.

5 N. Dan, Transport and Release in Nano-Carriers for Food Applications, *J. Food Eng.*, 2016, **175**, 136–144, DOI: **10.1016/j.jfoodeng.2015.12.017**.

6 S. Rodrigues, A. Avellan, G. D. Bland, M. C. R. Miranda, C. Larue, M. Wagner, D. A. Moreno-Bayona, H. Castillo-Michel, G. V. Lowry and S. M. Rodrigues, Effect of a Zinc Phosphate Shell on the Uptake and Translocation of Foliarly Applied ZnO Nanoparticles in Pepper Plants (*Capsicum Annuum*), *Environ. Sci. Technol.*, 2024, **58**, 3213–3223, DOI: **10.1021/acs.est.3c08723**.

7 N. C. Madlala, N. Khanyile and A. Masenya, Examining the Correlation between the Inorganic Nano-Fertilizer Physical Properties and Their Impact on Crop Performance and Nutrient Uptake Efficiency, *Nanomaterials*, 2024, **14**, 1263, DOI: **10.3390/nano14151263**.

8 E. Spielman-Sun, E. Lombi, E. Donner, D. Howard, J. M. Unrine and G. V. Lowry, Impact of Surface Charge on Cerium Oxide Nanoparticle Uptake and Translocation by Wheat (*Triticum Aestivum*), *Environ. Sci. Technol.*, 2017, **51**, 7361–7368, DOI: **10.1021/acs.est.7b00813**.

9 K. Ristroph, Y. Zhang, V. Nava, J. Wielinski, H. Kohay, A. M. Kiss, J. Thieme and G. V. Lowry, Flash NanoPrecipitation as an Agrochemical Nanocarrier Formulation Platform: Phloem Uptake and Translocation after Foliar Administration, *ACS Agric. Sci. Technol.*, 2023, **3**, 987–995, DOI: **10.1021/acsagscitech.3c00204**.

10 A. Avellan, J. Yun, Y. Zhang, E. Spielman-Sun, J. M. Unrine, J. Thieme, J. Li, E. Lombi, G. Bland and G. V. Lowry, Nanoparticle Size and Coating Chemistry Control Foliar Uptake Pathways, Translocation, and Leaf-to-Rhizosphere Transport in Wheat, *ACS Nano*, 2019, **13**, 5291–5305, DOI: **10.1021/acsnano.8b09781**.

11 S. Jeon, Y. Zhang, C. Castillo, V. Nava, K. Ristroph, B. Therrien, L. Meza, G. V. Lowry and J. P. Giraldo, Targeted Delivery of Sucrose-Coated Nanocarriers with Chemical Cargoes to the Plant Vasculature Enhances Long-Distance Translocation, *Small*, 2023, **20**(7), 2304588, DOI: **10.1002/smll.202304588**.

12 J. Zhu, J. Li, Y. Shen, S. Liu, N. Zeng, X. Zhan, J. C. White, J. Gardea-Torresdey and B. Xing, Mechanism of Zinc Oxide Nanoparticle Entry into Wheat Seedling Leaves, *Environ. Sci.: Nano*, 2020, **7**, 3901–3913, DOI: **10.1039/D0EN00658K**.

13 X. Gao, A. Kundu, D. P. Persson, A. Szameitat, F. Minutello, S. Husted and S. Ghoshal, Application of ZnO Nanoparticles Encapsulated in Mesoporous Silica on the Abaxial Side of a *Solanum Lycopersicum* Leaf Enhances Zn Uptake and Translocation via the Phloem, *Environ. Sci. Technol.*, 2023, **57**, 21704–21714, DOI: **10.1021/acs.est.3c06424**.

14 G. V. Lowry, J. P. Giraldo, N. F. Steinmetz, A. Avellan, G. S. Demirer, K. D. Ristroph, G. J. Wang, C. O. Hendren, C. A. Alabi and A. Caparco, *et al.* Towards Realizing Nano-Enabled Precision Delivery in Plants, *Nat. Nanotechnol.*, 2024, **19**, 1255–1269, DOI: **10.1038/s41565-024-01667-5**.

15 G. Mishra, B. Dash and S. Pandey, Layered Double Hydroxides: A Brief Review from Fundamentals to Application as Evolving Biomaterials, *Appl. Clay Sci.*, 2018, **153**, 172–186, DOI: **10.1016/j.clay.2017.12.021**.

16 M. Shafigh, M. Hamidpour and G. Furrer, Zinc Release from Zn-Mg-Fe(III)-LDH Intercalated with Nitrate, Phosphate and Carbonate: The Effects of Low Molecular Weight Organic Acids, *Appl. Clay Sci.*, 2019, **170**, 135–142, DOI: **10.1016/j.clay.2019.01.016**.

17 P. Songkhum, T. Wuttikhun, N. Chanlek, P. Khemthong and K. Laohhasurayotin, Controlled Release Studies of Boron and Zinc from Layered Double Hydroxides as the

Micronutrient Hosts for Agricultural Application, *Appl. Clay Sci.*, 2018, **152**, 311–322, DOI: **10.1016/j.clay.2017.11.028**.

18 H. Wu, X. Wan, J. Niu, H. Xu, Y. Zhang, X. Xue, Y. Li, Q. Li, T. Lu and H. Yu, *et al.* Enhancing Lettuce Yield via Cu/Fe-Layered Double Hydroxide Nanoparticles Spraying, *J. Nanobiotechnol.*, 2023, **21**, 417, DOI: **10.1186/s12951-023-02178-6**.

19 C. Wang, H. Zhu, N. Li, Q. Wu, S. Wang, B. Xu, Y. Wang and H. Cui, Dinotefuran Nano-Pesticide with Enhanced Valid Duration and Controlled Release Properties Based on a Layered Double Hydroxide Nano-Carrier, *Environ. Sci.: Nano*, 2021, **8**, 3202–3210, DOI: **10.1039/D1EN00661D**.

20 C. Wang, F. Gao, C. Sun, Y. Shen, S. Zhan, X. Li, H. Cui, L. Duan, Y. Wang and Y. Wang, Self-Assembly of 1-Triacontanol onto Layered Doubled Hydroxide Nano-Carriers toward Sustainable Growth Regulation of Maize, *Environ. Sci.: Nano*, 2022, **9**, 797–804, DOI: **10.1039/D1EN00972A**.

21 C. Del Hoyo, Layered Double Hydroxides and Human Health: An Overview, *Appl. Clay Sci.*, 2007, **36**, 103–121, DOI: **10.1016/j.clay.2006.06.010**.

22 V. B. Koman, M. Park, T. T. S. Lew, S. Wan, E. S. Yarwood, X. Gong, T. S. Shikdar, R. J. Oliver, J. Cui and P. Gordiichuk, *et al.* Emerging Investigator Series: Linking Nanoparticle Infiltration and Stomatal Dynamics for Plant Nanobionics, *Environ. Sci.: Nano*, 2022, **9**, 1236–1246, DOI: **10.1039/D1EN01154E**.

23 M. Y. Ghotbi, M. Z. Hussein, A. H. Yahaya and M. Z. A. Rahman, LDH-Intercalated d-Gluconate: Generation of a New Food Additive-Inorganic Nanohybrid Compound, *J. Phys. Chem. Solids*, 2009, **70**, 948–954, DOI: **10.1016/j.jpcs.2009.05.007**.

24 S. López-Rayo, A. Imran, H. C. Bruun Hansen, J. K. Schjoerring and J. Magid, Layered Double Hydroxides: Potential Release-on-Demand Fertilizers for Plant Zinc Nutrition, *J. Agric. Food Chem.*, 2017, **65**, 8779–8789, DOI: **10.1021/acs.jafc.7b02604**.

25 C.-M. Geilfus, L. Wang, J. Wu and C. Xue, The PH of the Leaf Apoplast Is Critical for the Formation of Pseudomonas Syringae-Induced Lesions on Leaves of the Common Bean (Phaseolus Vulgaris), *Plant Sci.*, 2020, **290**, 110328, DOI: **10.1016/j.plantsci.2019.110328**.

26 T. J. Monaco, S. C. Weller and F. M. Ashton, *Weed Science Principles and Practices*, Wiley, 2002, ISBN 978–0–471-37051-2.

27 D. Liang, C. Xia, H. Huang, Y. Liu, Z. Ma, S. Li, Q. Zhang and Z. Meng, Weed Control and Slow-Release Behavior of 2-Methyl-4-Chlorophenoxyacetate Intercalated Layered Double Hydroxide, *Colloids Surf., A*, 2023, **658**, 130661, DOI: **10.1016/j.colsurfa.2022.130661**.

28 P. P. Nadiminti, H. Sharma, S. R. Kada, F. M. Pfeffer, L. A. O'Dell and D. M. Cahill, Use of Mg–Al Nanoclay as an Efficient Vehicle for the Delivery of the Herbicide 2,4-Dichlorophenoxyacetic Acid, *ACS Sustainable Chem. Eng.*, 2019, **7**, 10962–10970, DOI: **10.1021/acssuschemeng.9b02001**.

29 R. G. Jain, S. J. Fletcher, N. Manzie, K. E. Robinson, P. Li, E. Lu, C. A. Brosnan, Z. P. Xu and N. Mitter, Foliar Application of Clay-Delivered RNA Interference for Whitefly Control, *Nat. Plants*, 2022, **8**(5), 535–548, DOI: **10.1038/s41477-022-01152-8**.

30 J. Yong, M. Wu, R. Zhang, S. Bi, C. W. G. Mann, N. Mitter, B. J. Carroll and Z. P. Xu, Clay Nanoparticles Efficiently Deliver Small Interfering RNA to Intact Plant Leaf Cells, *Plant Physiol.*, 2022, **190**, 2187–2202, DOI: **10.1093/PLPHYS/KIAC430**.

31 E. Spielman-Sun, A. Avellan, G. D. Bland, E. T. Clement, R. V. Tappero, A. S. Acerbo and G. V. Lowry, Protein Coating Composition Targets Nanoparticles to Leaf Stomata and Trichomes, *Nanoscale*, 2020, **12**, 3630–3636, DOI: **10.1039/C9NR08100C**.

32 A. Avellan, J. Yun, B. P. Morais, E. T. Clement, S. M. Rodrigues and G. V. Lowry, Critical Review: Role of Inorganic Nanoparticle Properties on Their Foliar Uptake and in Planta Translocation, *Environ. Sci. Technol.*, 2021, **55**, 13417–13431, DOI: **10.1021/ACS.EST.1C00178**.

33 M. El-Shetehy, A. Moradi, M. Maceroni, D. Reinhardt, A. Petri-Fink, B. Rothen-Rutishauser, F. Mauch and F. Schwab, Silica Nanoparticles Enhance Disease Resistance in Arabidopsis Plants, *Nat. Nanotechnol.*, 2021, **16**, 344–353, DOI: **10.1038/s41565-020-00812-0**.

34 Y. Shen, J. Borgatta, C. Ma, G. Singh, C. Tamez, N. P. Schultes, Z. Zhang, O. P. Dhankher, W. H. Elmer and L. He, *et al.*, Role of Foliar Biointerface Properties and Nanomaterial Chemistry in Controlling Cu Transfer into Wild-Type and Mutant Arabidopsis Thaliana Leaf Tissue, *J. Agric. Food Chem.*, 2022, **70**, 4267–4278, DOI: **10.1021/acs.jafc.1c07873**.

35 L. Stolte Bezerra Lisboa Oliveira and K. D. Ristroph, Critical Review: Uptake and Translocation of Organic Nanodelivery Vehicles in Plants, *Environ. Sci. Technol.*, 2024, **58**, 5646–5669, DOI: **10.1021/acs.est.3c09757**.

36 J. A. Heredia-Guerrero, J. J. Benítez, E. Domínguez, I. S. Bayer, R. Cingolani, A. Athanassiou and A. Heredia, Infrared and Raman Spectroscopic Features of Plant Cuticles: A Review, *Front. Plant Sci.*, 2014, **5**, 305, DOI: **10.3389/FPLS.2014.00305/BIBTEX**.

37 J. N. Henningsen, H. A. Bahamonde, K. H. Mühling and V. Fernández, Tomato and Pepper Leaf Parts Contribute Differently to the Absorption of Foliar-Applied Potassium Dihydrogen Phosphate, *Plants*, 2023, **12**, 2152, DOI: **10.3390/plants12112152**.

38 L. Rossi, L. N. Fedenia, H. Sharifan, X. Ma and L. Lombardini, Effects of Foliar Application of Zinc Sulfate and Zinc Nanoparticles in Coffee (Coffea Arabica L.) Plants, *Plant Physiol. Biochem.*, 2019, **135**, 160–166, DOI: **10.1016/J.PLAPHY.2018.12.005**.

39 H. Wu, N. Tito and J. P. Giraldo, Anionic Cerium Oxide Nanoparticles Protect Plant Photosynthesis from Abiotic Stress by Scavenging Reactive Oxygen Species, *ACS Nano*, 2017, **11**, 11283–11297, DOI: **10.1021/ACSNANO.7B05723/ASSET/IMAGES/NN-2017-05723R_M007.GIF**.

40 J. Zhu, J. Li, Y. Shen, S. Liu, N. Zeng, X. Zhan, J. C. White, J. Gardea-Torresdey and B. Xing, Mechanism of Zinc Oxide Nanoparticle Entry into Wheat Seedling Leaves, *Environ. Sci.: Nano*, 2020, **7**, 3901–3913, DOI: **10.1039/d0en00658k**.

41 Y. Du, P. Li, A. V. Nguyen, Z. P. Xu, D. Mulligan and L. Huang, Zinc Uptake and Distribution in Tomato Plants in Response to Foliar Supply of Zn Hydroxide-Nitrate Nanocrystal Suspension

with Controlled Zn Solubility, *J. Plant Nutr. Soil Sci.*, 2015, **178**, 722–731, DOI: **10.1002/jpln.201400213**.

42 I. Pacheco and C. Buzea, Nanoparticle Uptake by Plants: Beneficial or Detrimental? in *Phytotoxicity of Nanoparticles*, Springer International Publishing: Cham, 2018, pp. 1–61.

43 L. Zhao, T. Bai, H. Wei, J. L. Gardea-Torresdey, A. Keller and J. C. White, Nanobiotechnology-Based Strategies for Enhanced Crop Stress Resilience, *Nat. Food*, 2022, **2022**, 1–8, DOI: **10.1038/s43016-022-00596-7**.

44 M. Ishfaq, Y. Wang, M. Yan, Z. Wang, L. Wu, C. Li and X. Li, Physiological Essence of Magnesium in Plants and Its Widespread Deficiency in the Farming System of China, *Front. Plant Sci.*, 2022, **13**, 802274, DOI: **10.3389/fpls.2022.802274**.

45 A. H. Chaudhry, S. Nayab, S. B. Hussain, M. Ali and Z. Pan, Current Understandings on Magnesium Deficiency and Future Outlooks for Sustainable Agriculture, *Int. J. Mol. Sci.*, 2021, **22**, 1819, DOI: **10.3390/ijms22041819**.

46 A. Maillard, S. Diquélou, V. Billard, P. Laîné, M. Garnica, M. Prudent, J.-M. Garcia-Mina, J.-C. Yvin and A. Ourry, Leaf Mineral Nutrient Remobilization during Leaf Senescence and Modulation by Nutrient Deficiency, *Front. Plant Sci.*, 2015, **6**, 1–15, DOI: **10.3389/fpls.2015.00317**.

47 Y. Kuroda, Y. Miyamoto, M. Hibino, K. Yamaguchi and N. Mizuno, Tripodal Ligand-Stabilized Layered Double Hydroxide Nanoparticles with Highly Exchangeable $CO32^{-}$, *Chem. Mater.*, 2013, **25**, 2291–2296, DOI: **10.1021/cm400846k**.

48 C. E. Markwalter, R. F. Pagels, B. K. Wilson, K. D. Ristroph and Prud'homme, R.K., Flash NanoPrecipitation for the Encapsulation of Hydrophobic and Hydrophilic Compounds in Polymeric Nanoparticles, *J. Visualized Exp.*, 2019, **143**, e58757, DOI: **10.3791/58757**.

49 J. Wielinski, X. Huang and G. V. Lowry, Characterizing the Stoichiometry of Individual Metal Sulfide and Phosphate Colloids in Soils, Sediments, and Industrial Processes by Inductively Coupled Plasma Time-of-Flight Mass Spectrometry, *Environ. Sci. Technol.*, 2024, **58**, 12113–12122, DOI: **10.1021/acs.est.3c10186**.

50 H. E. Pace, N. J. Rogers, C. Jarolimek, V. A. Coleman, C. P. Higgins and J. F. Ranville, Determining Transport Efficiency for the Purpose of Counting and Sizing Nanoparticles via Single Particle Inductively Coupled Plasma Mass Spectrometry, *Anal. Chem.*, 2011, **83**, 9361–9369, DOI: **10.1021/ac201952t**.

51 M. Tanner and D. Günther, Short Transient Signals, a Challenge for Inductively Coupled Plasma Mass Spectrometry, a Review, *Anal. Chim. Acta*, 2009, **633**, 19–28, DOI: **10.1016/j.aca.2008.11.041**.

52 Y. Shen, J. Borgatta, C. Ma, W. Elmer, R. J. Hamers and J. C. White, Copper Nanomaterial Morphology and Composition Control Foliar Transfer through the Cuticle and Mediate Resistance to Root Fungal Disease in Tomato (*Solanum Lycopersicum*), *J. Agric. Food Chem.*, 2020, **68**, 11327–11338, DOI: **10.1021/acs.jafc.0c04546**.

53 Z. Xu and G. Zhou, Responses of Leaf Stomatal Density to Water Status and Its Relationship with Photosynthesis in a Grass, *J. Exp. Bot.*, 2008, **59**, 3317–3325, DOI: **10.1093/jxb/ern185**.

54 P. P. Nadiminti, J. E. Rookes, B. J. Boyd and D. M. Cahill, Confocal Laser Scanning Microscopy Elucidation of the Micromorphology of the Leaf Cuticle and Analysis of Its Chemical Composition, *Protoplasma*, 2015, **252**, 1475–1486, DOI: **10.1007/S00709-015-0777-6**.

55 Y. Zhang, L. Fu, S. J. Jeon, J. Yan, J. P. Giraldo, K. Matyjaszewski, R. D. Tilton and G. V. Lowry, Star Polymers with Designed Reactive Oxygen Species Scavenging and Agent Delivery Functionality Promote Plant Stress Tolerance, *ACS Nano*, 2022, **16**, 4467–4478, DOI: **10.1021/acsnano.1c10828**.

56 E. Domínguez, J. A. Heredia-Guerrero and A. Heredia, The Biophysical Design of Plant Cuticles: An Overview, *New Phytol.*, 2011, **189**, 938–949, DOI: **10.1111/j.1469-8137.2010.03553.x**.

57 M. Ádok-Sipiczki, I. Szilagyi, I. Pálinkó, M. Pavlovic, P. Sipos and C. Nardin, Design of Nucleic Acid-Layered Double Hydroxide Nanohybrids, *Colloid Polym. Sci.*, 2017, **295**, 1463–1473, DOI: **10.1007/s00396-017-4122-9**.

58 S. Agarwal, D. K. Jangir, R. Mehrotra, N. Lohani and M. R. Rajeswari, A Structural Insight into Major Groove Directed Binding of Nitrosourea Derivative Nimustine with DNA: A Spectroscopic Study, *PLoS One*, 2014, **9**, e104115, DOI: **10.1371/journal.pone.0104115**.

59 P. Hu, J. An, M. M. Faulkner, H. Wu, Z. Li, X. Tian and J. P. Giraldo, Nanoparticle Charge and Size Control Foliar Delivery Efficiency to Plant Cells and Organelles, *ACS Nano*, 2020, **14**, 7970–7986, DOI: **10.1021/acsnano.9b09178**.

60 S. Husted, F. Minutello, A. Pinna, S. Tougaard, P. Møs and P. M. Kopittke, What Is Missing to Advance Foliar Fertilization Using Nanotechnology?, *Trends Plant Sci.*, 2023, **28**, 90–105.

61 S. Husted, F. Minutello, A. Pinna, S. Tougaard, P. Møs and P. M. Kopittke, What Is Missing to Advance Foliar Fertilization Using Nanotechnology?, *Trends Plant Sci.*, 2023, **28**, 90–105.

62 H. Zhang, N. S. Goh, J. W. Wang, R. L. Pinals, E. González-Grandío, G. S. Demirer, S. Butrus, S. C. Fakra, A. Del Rio Flores and R. Zhai, *et al.* Nanoparticle Cellular Internalization Is Not Required for RNA Delivery to Mature Plant Leaves, *Nat. Nanotechnol.*, 2022, **17**, 197–205, DOI: **10.1038/s41565-021-01018-8**.

63 G. C. Arya, S. Sarkar, E. Manasherova, A. Aharoni and H. Cohen, The Plant Cuticle: An Ancient Guardian Barrier Set Against Long-Standing Rivals, *Front. Plant Sci.*, 2021, **12**, 1264.

64 V. Saharan, G. Sharma, M. Yadav, M. K. Choudhary, S. S. Sharma, A. Pal, R. Raliya and P. Biswas, Synthesis and in Vitro Antifungal Efficacy of Cu–Chitosan Nanoparticles against Pathogenic Fungi of Tomato, *Int. J. Biol. Macromol.*, 2015, **75**, 346–353, DOI: **10.1016/j.ijbiomac.2015.01.027**.

65 P. Patel, P. Kumar Jatav, R. Jain, S. Gupta, S. Kothari and S. Kachhwaha, Humidity Induced Opening of Stomata Leads to Enhanced Uptake of Copper Nanoparticles in Triticum Aestivum L, *Mater. Today: Proc.*, 2021, **43**, 3191–3196, DOI: **10.1016/j.matpr.2021.01.712**.

66 W. L. Araújo, A. R. Fernie and A. Nunes-Nesi, Control of Stomatal Aperture, *Plant Signaling Behav.*, 2011, **6**, 1305–1311, DOI: **10.4161/psb.6.9.16425**.

67 J. Burkhardt, S. Basi, S. Pariyar and M. Hunsche, Stomatal Penetration by Aqueous Solutions – an Update Involving Leaf Surface Particles, *New Phytol.*, 2012, **196**, 774–787, DOI: **10.1111/j.1469-8137.2012.04307.x**.

68 H. Xu, Z. Luo, W. Hu, Y. Jia, Y. Wang, X. Ye, Y. Li, L.-S. Chen and J. Guo, Magnesium Absorption, Translocation, Subcellular Distribution and Chemical Forms in Citrus Seedlings, *Tree Physiol.*, 2022, **42**, 862–876, DOI: **10.1093/treephys/tpab148**.

69 M. L. Parello, R. Rojas and C. E. Giacomelli, Dissolution Kinetics and Mechanism of Mg-Al Layered Double Hydroxides: A Simple Approach to Describe Drug Release in Acid Media, *J. Colloid Interface Sci.*, 2010, **351**, 134–139, DOI: **10.1016/j.jcis.2010.07.053**.

70 W. F. Falco, M. D. Scherer, S. L. Oliveira, H. Wender, I. Colbeck, T. Lawson and A. R. L. Caires, Phytotoxicity of Silver Nanoparticles on Vicia Faba: Evaluation of Particle Size Effects on Photosynthetic Performance and Leaf Gas Exchange, *Sci. Total Environ.*, 2020, **701**, 134816, DOI: **10.1016/j.scitotenv.2019.134816**.

71 H. Lambers, F. S. Chapin and T. L. Pons, Photosynthesis. in *Plant Physiological Ecology*, Springer: New York, 2008, pp. 11–99.

72 J. Yang, W. Cao and Y. Rui, Interactions between Nanoparticles and Plants: Phytotoxicity and Defense Mechanisms, *J. Plant Interact.*, 2017, **12**, 158–169, DOI: **10.1080/17429145.2017.1310944**.

